

UKAEA-CCFE-PR(20)115

R. Worrall, B. Colling, M. R. Gilbert, E. Litherland-Smith, C. R. Nobs, L. W. Packer, C. Wilson, A. Zohar

Deformation heterogeneity in laser-welded Eurofer

Enquiries about copyright and reproduction should in the first instance be addressed to the UKAEA Publications Officer, Culham Science Centre, Building K1/O/83 Abingdon, Oxfordshire, OX14 3DB, UK. The United Kingdom Atomic Energy Authority is the copyright holder.

The contents of this document and all other UKAEA Preprints, Reports and Conference Papers are available to view online free at scientific-publications.ukaea.uk/

Deformation heterogeneity in laser-welded Eurofer

R. Worrall, B. Colling, M. R. Gilbert, E. Litherland-Smith, C. R. Nobs, L. W. Packer, C. Wilson, A. Zohar

The development, testing and comparison of unfolding methods in SPECTRA-UF for neutron spectrometry

R. Worrall^{a,*}, B. Colling^a, M. R. Gilbert^a, E. Litherland-Smith^a, C. R. Nobs^a, L. W. Packer^a, C. Wilson^a and A. Zohar^b

^aUnited Kingdom Atomic Energy Authority, Culham Centre for Fusion Energy, Culham Science Centre, Abingdon, Oxon, OX14 3DB, UK

^bJozef Stefan Institute - Reactor Physics Department, Jamova cesta 39, SI-1000 Ljubljana, Slovenia

ARTICLE INFO

Keywords:

Neutron spectrometry
Spectrum unfolding
Activation Foil
GRAVEL
MAXED
Parameterised spectrum features
SPECTRA-UF

ABSTRACT

Spectrum unfolding is a key tool used together with diagnostics in the determination of nuclear fields that are associated with a range of nuclear technologies spanning fusion, fission, nuclear medicine and accelerator domains. The underlying process requires a mathematical method for solving the Fredholm integral equation of the first kind. This paper discusses the development, testing and comparison of the modern combined framework of methods for performing neutron spectrum unfolding SPECTRA-UF, which includes the UF_G and UF_M subroutines, based on the underlying mathematics of the GRAVEL and MAXED methods respectively, along with a custom parameterised subroutine, UF_P. We compared the behaviour of each method using a set of synthetic data. We discuss the challenges associated with unfolding fusion spectra, and the behaviour of each subroutine along with the feasibility of using general parameterised spectra as initial *a priori* spectra. The UF_M, UF_G and UF_P methods showed reasonable agreement where good *a priori* was supplied and all improved on the *a priori* spectrum given, but behaved poorly where less accurate *a priori* was provided, with UF_G showing itself to rely more heavily on the *a priori* spectrum given. The UF_M subroutine performed most favourably, producing the lowest mean fractional deviation across the majority of spectra. The UF_P was able to represent the fusion peaks and relatively smooth epi-thermal regions, but performed less well where the flux spanned many orders of magnitude. The modelling of the down-scatter component of the fusion peaks was also challenging to reliably model using simple distributions.

1. Introduction

The neutron energy spectra within a fusion device are difficult to measure, due partly to the indirect nature of measuring neutrons but also the extremes in temperature, electromagnetic fields and high neutron and photon fluxes found in fusion environments. These extremes make the use of sensitive electronics highly challenging in some locations and impossible in others, such as at the first wall or in the breeder blankets. The accurate knowledge of the neutron field is essential for a wide range of applications such as the inference of plasma parameters, material behaviour, safety factors and tritium breeding ratios. Dosimetry foils are well known for their nuclear resilience [24, 17] and, in some cases, can be used in such environments; these consist of a set of materials that, when irradiated by neutrons, undergo various reactions producing daughter radioisotopes. The initial activity of the daughters can be inferred from the measurement of the decay radiation using gamma-ray spectrometers. Provided the reaction rate response of each isotope to neutrons is known for each reaction channel, the neutron flux incident to the foil can be estimated using an unfolding method. However, the number of measurable reactions are limited by a number of physical requirements such as half-life, gamma energy, emission probability and constrained by the length of irradiation and time between extraction and measurement. Where activation foils have fewer reaction channels than en-

ergy channels, an infinite number of possible solution spectra may exist, which makes the unfolding process and error propagation challenging.

This work describes the development, testing and comparison of a combined framework of unfolding methods for use with neutron spectrometry, describing the underlying mathematics of each method implemented and comparing the behaviour and accuracy of each method by applying a synthetic data set comprising spectra from various fusion environments.


Neutron spectrum unfolding using dosimetry foils is described by a set of Fredholm integral equations of the first kind. The reaction rates during irradiation in each of the i^{th} reaction channels, Z_{0i} , are represented in equation 1, where the response of each reaction channel, $R_i(E)$, is the reaction rate induced per unit of neutron flux, and $\Phi(E)$, is the neutron flux incident to the given foil.

Neutron spectrum unfolding using dosimetry foils is described by a set of Fredholm integral equations of the first kind. The reaction rates during irradiation in each of the i^{th} reaction channels, Z_{0i} , are represented in equation 1, where $R_i(E)$ is the total reaction rate for reaction channel i at energy E in units of barns per neutron per second and $\phi(E)$ is the neutron flux ($n\text{ cm}^{-2}\text{ s}^{-1}$) at energy E incident on the foil.

$$Z_{0i} = \int_0^{\infty} R_i(E)\Phi(E)dE, \quad i = 1, 2, \dots, m \quad (1)$$

Unfolding typically requires that equation 1 is represented

*Corresponding author

 ross.worrall@ukaea.uk (R. Worrall)

ORCID(s):

in a discretised form, with the flux in the j^{th} energy channel, Φ_j , and the response, $R_{i,j}$, shown in equation 2.

$$Z_{0i} = \sum_{j=1}^n R_{i,j} \Phi_j \quad j = 1, 2, \dots, n \quad (2)$$

This gives a set of equations with m reaction channels and a neutron spectrum with n energy channels. A unique solution to the neutron spectrum exists only if the number of unknown flux values (n) are equal to or less than the number of reaction channels (m). The response matrix must also be full rank as any vectors that are non-linearly independent will not provide any information and hence, reduce the amount of information available. Typically for fusion applications, and indeed in the cases we discussed in this paper, the number of measurable reaction channels are fewer than the number of energy channels ($m \ll n$) and thus, the system of equations will be an ill-conditioned and under-determined inverse problem with an infinite number of possible solutions.

2. Existing methods and codes

To aid in the analysis of various activation foil systems currently under development for fusion experiments, such as those being applied at the Joint European Torus (JET) and future application to ITER and DEMO, a range of unfolding methods have been integrated by UKAEA into a combined framework for neutron spectrometry. Many packages of codes exist, which take differing approaches to unfolding and can be designed for use with specific detectors or radiation environments. These packages are written in a variety of programming languages, and vary greatly in the required quantity and formatting of the input data files, and, especially with older codes, can require fixed width text files that are often time consuming to create. The developed framework is written using modern coding practices and aims to have a simple unified input and output format and uses only the core mathematical equations underpinning each unfolding method. This allows the user to conveniently access a range of possible solutions from independent algorithms as well as providing output information for each method such as the reduced χ^2 of the fitted reaction rates.

A wide range of unfolding methods have been written, some designed for use with ‘few-channel’ under-determined problems, such as with activation foils or Bonner sphere systems, and others for ‘multi-channel’ more fully determined problems, such as with gamma spectrometry or scintillation detectors. Examples of these are the non-linear least square iterative adjustment methods, such as SAND-II [14], GRAVEL [11] and SPUNIT [3], the entropy methods including MAXED [18], MIEKE and UNFANA [12], regularisation methods, such as LOUHI [19], parameterisation methods, and machine learning methods, such as genetic algorithms and artificial neural networks. Due to the often under-determined nature of the problem, many codes require prior information (*a priori*) to be provided, such as an initial guess spectrum, smoothing parameters or information about the phys-

ical nature of the system. Understanding the behaviour, reliability and limitations of each of these methods is of high importance for a user with an under-determined problem as each method must select a single suitable candidate spectrum from a possibly large solution space.

A range of unfolding code comparisons have been undertaken over the past few decades [1, 9, 22, 25], which mainly focus on fission reactors or environmental dosimetry using either Bonner sphere systems or dosimetry foils. Fusion spectra in comparison provide further challenges as the magnitude of the flux in each bin and the energy of the neutrons typically span many orders of magnitude, making the unfolding process challenging.

The foils may also be used in new devices, plasma campaigns or with novel experiments where there may be less pre-existing information compared with more well understood environments.

3. UKAEA unfolding code framework

The UKAEA unfolding framework SPECTRA-UF was developed using Python 3 to include a range of unfolding methods, along with post processing tools, such as a Monte Carlo error propagation method. The unfolding framework includes the subroutines UF_SA, UF_G, UF_SP and UF_M that are written based on the underlying mathematics of the SAND-II [14], GRAVEL [12], SPUNIT [3] and MAXED [18] methods respectively, along with a custom parameterised method, UF_P. The Monte Carlo method for error propagation allows the user to supply the uncertainties associated with any input vector or matrix, and stochastically varies the respective input values and records the distribution of solutions produced by each unfolding method, providing an estimate of uncertainty based on a confidence margin and tolerance specified by the user. This produces an associated uncertainty for any of the output vectors required, such as the uncertainty on each channel of the solution spectrum.

3.1. Subroutine UF_G based on GRAVEL

The UF_G algorithm uses the GRAVEL iterative method described by Matzke in the HEPROW package [12]. GRAVEL is a non-linear least square gradient descent method based on the SAND-II algorithm written by the USAF [14] and modified to include uncertainty weightings for the measured reaction rates. The iterative algorithm calculates the flux in logarithmic space to avoid generating a negative solution, as shown in equations 3 - 6 where the flux Φ_j at the $k+1^{th}$ step is calculated based on the flux at the previous k^{th} step, Z_{0i} and σ_{oi} are the measured reaction rates and their uncertainties respectively, and $Z_i^{(k)}$ are the calculated reaction rates for the solution at the k^{th} step. The reaction rate weighting matrix $\omega_{i,j}$, with the response matrix $R_{i,j}$ are shown in equation 5. The relative uncertainty of the reaction rates ρ_i is shown in equation 6.

The GRAVEL method only differs from the original SAND-II algorithm by the inclusion of the relative uncertainty term ρ_i . The algorithm SPUNIT [3] is based on a similar deriva-

tion to that of GRAVEL and produces almost identical results to the GRAVEL code. As the UF_SA and UF_SP are based on the underlying mathematics of the SAND-II and SPUNIT methods, and produce almost identical results to that of the UF_G subroutine, neither have been included in this study as they would produce almost identical results.

$$\ln \Phi^{(k+1)} = \ln \Phi_j^{(k)} + \lambda_j^{(k)} \sum_{i=1}^m \left[(\ln Z_{0i} - \ln Z_i^{(k)}) \frac{\omega_{i,j}^{(k)}}{\rho_i^2} \right] \quad (3)$$

$$\lambda_j^{(k)} = \left(\sum_{i=1}^m \frac{\omega_{i,j}^{(k)}}{\rho_i^2} \right)^{-1} \quad (4)$$

$$\omega_{i,j}^{(k)} = \frac{R_{i,j} \Phi_j^{(k)}}{Z_i^{(k)}} \quad (5)$$

$$\rho_i = \frac{\sigma_{0i}}{z_{0i}} \quad (6)$$

The GRAVEL algorithm makes the assumption that the distribution or ‘shape’ of the solution spectrum is close to that of the *a priori* spectrum. The algorithm will find a unique solution given an over-determined problem. However, in heavily under-determined problems, the solution spectrum will depend heavily on the *a priori* spectrum and it is not always transparent as to the level of influence this has on the solution spectrum. Thus care should be taken in choosing an initial guess spectrum. The *a priori* should be based on the known physical properties within the spectrum or ideally calculated using a Monte Carlo transport code.

The user can specify the convergence criteria for the UF_G subroutine, either running to a given number of iterations or until a reduced chi-squared value for the solution reaction rates is achieved.

During development and testing of the unfolding framework, the UF_G subroutine was compared to the UMG3.3 few channel version of GRAVEL using a range of test spectra and was found to produce almost identical results, with only small rounding errors accounting for these minute differences. The UF_G subroutine was also given an over-determined problem, with full rank response matrix where a unique solution exists and was able to converge on this solution given sufficient iterations.

3.2. Subroutine UF_M based on MAXED

The MAXED code was developed by Reginatto and Goldhagen [18] and uses the principles of maximum entropy to allow the inclusion of an *a priori* spectrum. The magnitude of the relative entropy between two discrete distributions gives a measure of the difference between the *a priori* spectrum, also known as the default spectrum Φ_j^{DEF} and the solution spectrum Φ_j , as shown in equation 7.

$$S = - \sum_{i=1}^m \left[\Phi_j \ln \left(\frac{\Phi_j}{\Phi_j^{DEF}} \right) + \Phi_j^{DEF} - \Phi_j \right] \quad (7)$$

Solution spectra are defined using two conditions, the matching of the empirical reaction rates Z_i given an unknown uncertainty ϵ_i , shown in equation 8, and the χ^2 statistic, shown in equation 9, where σ_i is the empirical uncertainty and Ω is a fitting parameter, typically set to the number of reaction channels.

$$Z_i + \epsilon_i = \sum_{j=1}^n R_{i,j} \Phi_j \quad i = 1, 2, \dots, m \quad (8)$$

$$\sum_{i=1}^m \frac{\epsilon_i^2}{\sigma_i^2} = \Omega \quad (9)$$

The Lagrangian associated with the maximisation of the relative entropy shown in equation 7, and given the constraints of equations 8 and 9 is shown in equation 10.

$$\begin{aligned} \mathcal{L}(\Phi_j, \epsilon_i, \lambda_i, \mu) = & - \sum_{j=1}^n \left[\Phi_j \ln \left(\frac{\Phi_j}{\Phi_j^{DEF}} \right) + \Phi_j^{DEF} - \Phi_j \right] \\ & - \sum_{i=1}^M \lambda_i \left(\sum_{j=1}^n R_{i,j} \Phi_j - N_i - \epsilon_i \right) - \mu \left[\sum_{i=1}^m \left(\frac{\epsilon_i}{\sigma_i} \right)^2 - \Omega \right] \end{aligned} \quad (10)$$

This leads to a set of equations with corresponding Lagrange multipliers λ , that can be reduced to form a potential function H , which when maximised will provide a solution spectrum.

$$\begin{aligned} H = & - \sum_{j=1}^n f_j^{DEF} \exp \left(- \sum_{i=1}^m \lambda_i R_{i,j} \right) \\ & - \left(\Omega \sum_{i=1}^m (\lambda_i \sigma_i)^2 \right)^{\frac{1}{2}} - \sum_{i=1}^m Z_i \lambda_i \end{aligned} \quad (11)$$

The user specifies the convergence criteria for the UF_M subroutine by setting the Ω term, shown in equation 9, as well as specifying the optimisation method used to find the parameters in equation 11, either using a Limited Memory Broyden-Fletcher-Goldfarb-Shanno (L-BFGS) [6] or a Basin Hopping [20] minimisation algorithm, where the solution spectrum depends on the *a priori* and λ parameters as shown in equation 12.

$$\Phi_j = \Phi_j^{DEF} \exp \left(- \sum_{i=1}^m \lambda_i R_{i,j} \right) \quad j = 1, \dots, n \quad (12)$$

During development and testing of the unfolding framework, the UF_M subroutine was compared to the UMG3.3 few channel version of MAXED and was found to produce similar results, with the differences being accounted for by the pre-processing of input data, such as in the way the *a priori* spectrum is normalised before the optimisation of the λ parameters described in equation 11.

3.3. Parameterised unfolding via subroutine UF_P

A parameterised method was written to approximate the physical features within a spectrum using a range of mathematical distributions, such as a Gaussian distribution (Φ_G) for each fusion peak, a Maxwellian distribution (Φ_M) for the thermalised peak found in water cooled breeder blankets and a set of log-normal distributions (Φ_L) to create flat regions in log-space to represent the down scattered neutrons. The sum of these continuous probability distributions form a total spectrum (Φ_{total}) as shown in equation 13. The total continuous spectrum is then discretised to form a spectrum that can be used during the unfolding process.

$$\Phi_{\text{total}} = \sum_i^m \Phi_{G,i} + \sum_j^n \Phi_{M,j} + \sum_k^o \Phi_{L,k} \quad (13)$$

For each of the Gaussian distributions ($\Phi_{G,i}$), the user can set the i^{th} mean (μ_i) and variance (σ_i) shown in equation 14 where E is the energy, and can set the mean to be either a fixed or free parameter.

$$\Phi_{G,i}(E) = \frac{1}{\sigma_i \sqrt{2\pi}} \exp\left(-\frac{1}{2}\left(\frac{E - \mu_i}{\sigma_i}\right)^2\right) \quad (14)$$

For each of the Maxwellian distributions ($\Phi_{M,j}$) the user can set the j^{th} parameter a_j , which represents the mode over $\sqrt{2}$ as shown in equation 15, where E is the energy.

$$\Phi_{M,j}(E) = \sqrt{\frac{2}{\pi}} \frac{E^2 \exp\left(-\frac{E^2}{2a_j^2}\right)}{a_j^3} \quad (15)$$

The number of log-normal distributions that comprise the logarithmically spaced series Φ_L can be defined by the user, along with the mode of the lowest and highest energy peak and a parameter which defines the relative widths of each peak in log-space. The subroutine generates a logarithmically spaced series of log-normal distributions, and calculates the mean (μ_l) and width parameter (σ_l) for each of the l^{th} log-normal distributions, as shown in equation 16 where E is the energy. The user can set the mean of all the log-normal distributions to be either fixed or a free parameters.

$$\Phi_{L,k}(E) = \sum_l^p \frac{1}{E \sigma_l \sqrt{2\pi}} \exp\left(-\frac{(\ln E - \mu)^2}{2\sigma_l^2}\right) \quad (16)$$

The user specifies the convergence criteria for the UF_P subroutine by setting the reduced chi-squared of the fitted reaction rates, as well as specifying the optimisation method used to find the free parameters within each distribution, either using a Limited Memory Broyden-Fletcher-Goldfarb-Shanno (L-BFGS) [6] or a Basin Hopping [20] minimisation algorithm.

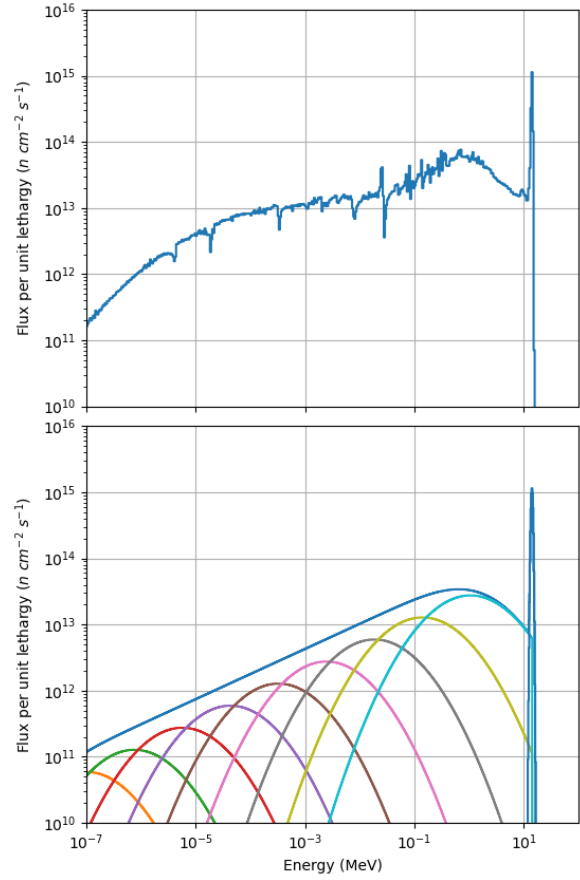


Figure 1: Example of the distributions within a parameterised DT spectrum. Top, shows the target spectrum at the first wall of a 'DT water-cooled LiPb concept' [23]. Bottom, shows a parameterised approximation of the top spectrum, with a logarithmically distributed set of log-normal probability density functions and a Gaussian to represent the DT peak.

An example parameterised DT spectrum is shown in figure 1. Each distribution defined by the user is generated within the group structure given and summed together to form a spectrum. The subroutine is then able to change all or some of the parameters of each distribution, such as the width and amplitude of a Gaussian with a fixed mean or mode at a known energy peak.

4. Synthetic data and comparison of methods

A set of 415 fusion spectra were taken from theoretically simulated data for the JET, ITER and DEMO reactors and were chosen to represent a wide range of fusion environments, fuel types and positions within a device. These were comprised of reference spectra [10, 23] generated using models of the JET, ITER and DEMO fusion devices and

Table 1
Description of each category of spectra.

| Category | Description | Spectra included |
|---------------------|--|------------------|
| DT FW | First wall of the JET, ITER and DEMO devices during DT operation | 7 |
| DD | First wall of the ITER device during DD operation | 1 |
| DT VV No water | Outer wall of vacuum vessel in the DEMO device during DT operations | 3 |
| DT VV with water | Outer wall of vacuum vessel with water cooled breeder blankets in the DEMO device during DT operations | 2 |
| DD KN1 | Outside of the vacuum vessel in the JET device during DD operations | 4 |
| DT KN1 | Outside of the vacuum vessel in the JET device during DT operations | 4 |
| TT KN1 | Outside of the vacuum vessel in the JET device during TT operations | 4 |
| DD KN2/OLTIS | First wall of the JET device during DD operations | 130 |
| DT KN2/OLTIS | First wall of the JET device during DT operations | 130 |
| TT KN2/OLTIS | First wall of the JET device during TT operations | 130 |

simulated using the Monte Carlo N-Particle transport code (MCNP) for a range of device configurations. Each spectrum was folded with the response matrix to form a set of synthetic reaction rates, with these and an *a priori* spectrum given to each subroutine. The spectra were categorised by their position within the reactor, the type of fusion reaction undertaken including deuterium-deuterium (DD), deuterium-tritium (DT) or tritium-tritium (TT), and by physical attributes such as thermal peaks caused by water moderation. A description of these categories is shown in table 1. An *a priori* spectrum was created for each category using UF_P, with a peak for either the DD, DT or TT peak, a sloped region made of equally log-spaced log-normal distributions and a Maxwellian peak if significant thermalisation is present. A logarithmically spaced set of log-normal distributions was used rather than a straight line in log-log space as it better describes the typically curved intermediate region which lies between the fusion peak and the thermal region. No uncertainties were propagated with the results as none were introduced into the synthetic data set. However, arbitrarily selected uncertainties of 2 % were given as inputs for the UF_G and UF_M subroutines.

The selected elements used in the response matrix were

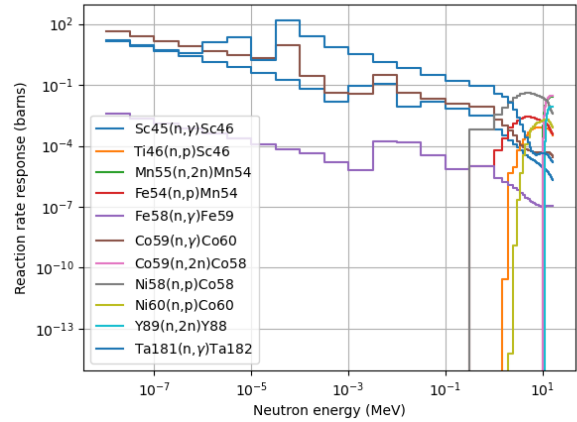


Figure 2: Response matrix reaction channels

based on foils found commonly in activation systems currently under development, such as the the noVel nEutRon Detector for fusion (VERDI) [16] and the JET Test Blanket Module Development (TBMD) [7] detector systems, as shown in table 2. The synthetic response matrix was created using the ENDF/B-VIII.0 nuclear data library [4], with the response in each reaction channel scaled to an arbitrary volume. Figure 2 shows a plot of the response in each reaction channel.

Table 2

Selected dosimetry reactions used to form the synthetic response matrix. E_γ is the principle γ emission line energy and E_{th} is the approximate energy threshold of the reaction [2, 5, 8, 13, 15, 21, 26]

| Parent isotope | Half-life | E_γ (MeV) | E_{th} (MeV) |
|--------------------------|-----------|------------------|----------------|
| Sc45(n, γ)Sc46 | 84 d | 0.98, 1.12 | - |
| Ti46(n,p)Sc46 | 84 d | 0.98, 1.12 | 1.7 |
| Mn55(n,2n)Mn54 | 312 d | 0.83 | 10.6 |
| Fe54(n,p)Mn54 | 312 d | 0.83 | 0.7 |
| Fe58(n, γ)Fe59 | 44 d | 1.10 | - |
| Co59(n, γ)Co60 | 1925 d | 1.17, 1.33 | - |
| Co59(n,2n)Co58 | 71 d | 0.81 | 10.7 |
| Ni58(n,p)Co58 | 71 d | 0.81 | 0.5 |
| Ni60(n,p)Co60 | 1925 d | 1.17, 1.33 | 2.1 |
| Y89(n,2n)Y88 | 106 d | 1.84 | 12.0 |
| Ta181(n, γ)Ta182 | 115 d | 1.12 | - |

The selected custom energy group structure consists of 56 bins, with 16 logarithmically spaced energy bins from 10^{-7} up to 1 MeV and a further 40 finer resolution linearly spaced bins up to 20 MeV. The logarithmically distributed bins at lower energies were chosen to reflect the unequal distribution of information across the energy range stored in a set of reaction rates and response matrix. This switch to a linear distribution is primarily due to the majority of reactions having energy thresholds typically greater than 1 MeV, as below the threshold energy no reaction occurs and hence, no information is stored. Another contributing factor

which exacerbates the lack of information at lower energies is the problem with non-linear independence. This may occur when the relatively few responses of the non-threshold reactions have a similar $1/v$ shape common to capture reactions in non-resonance regions, which may cause the column vectors within the response matrix to approach non-linear independence; that is, the values within the column vectors will approach the same ratio as one another, thus, making two energy channels indistinguishable.

The convergence criteria for each unfolding method differs in definitions, making a consistent set of input parameters impossible. However, each method allows the user to either directly or indirectly specify the desired reduced χ^2 of the fitted reaction rates. The target reduced χ^2 was set to unity directly in the UF_G and UF_P methods, and indirectly by setting the Ω parameters to the number of reaction channels in UF_M.

5. Results of comparison and discussion

Solution spectra produced by each unfolding method were compared with their respective target spectra, with results being split into three broad energy regions of interest to allow broad comparisons to be made between spectra: a region covering thermalisation up to 10^{-5} MeV, an intermediate region between 10^{-5} and 1 MeV, and a fast region from 1 MeV to 20 MeV. The integrated flux across each energy region was compared to those of the target spectra, with results shown in table 3. The fractional deviation of the solution flux from their respective target flux was calculated for each energy channel, with the mean of the fractional deviation across all energy bins within all spectra shown in table 4, and the mean of the fractional deviation across all energy bins within spectra in each category shown in table 5, each of which are also broken down by energy region.

Table 3

The mean percentage deviation of the integrated flux in each energy region of the solution from the target spectra, averaged across all spectra.

| | 0 - 10^{-5} MeV | 10^{-5} - 1 MeV | 1 - 20 MeV | Total |
|-----------------|-------------------|-------------------|------------|--------|
| UF_M | 14.5% | 7.7% | 22.1% | 11.3 % |
| UF_G | 42.5% | 10.3% | 22.6% | 12.6 % |
| UF_P | 36.4% | 5.3% | 15.5% | 8.3 % |
| <i>A priori</i> | 146.7% | 20.0% | 18.5% | 11.3 % |

The convergence criteria for each method was set to a target reduced χ^2 for the fitted reactions rates of unity. However, due to the differing methodologies the subroutines compared tended to either over or under fit to a small degree. The UF_G method is iterative and takes discrete steps through the solution space, with the reduced χ^2 being calculated after each iteration, and hence, a reduced χ^2 of less than or equal to unity is always produced. UF_M uses a stochastic optimisation method which searches through the solution space and converges towards a reduced χ^2 of unity, typically getting extremely close to this value. The UF_P also uses a

Table 4

The mean of the fractional deviation of the solution flux from the target flux across all energy channels and spectra.

| | 0 - 10^{-5} MeV | 10^{-5} - 1 MeV | 1 - 20 MeV | Total |
|-----------------|-------------------|-------------------|------------|-------|
| UF_M | 0.120 | 0.157 | 0.486 | 0.365 |
| UF_G | 12.342 | 0.355 | 0.454 | 2.021 |
| UF_P | 1.643 | 1.523 | 0.620 | 0.945 |
| <i>A priori</i> | 33.486 | 1.633 | 0.655 | 5.197 |

stochastic optimisation method, which will stop searching once either a reduced χ^2 of unity is reached or the rate of improvement falls below a threshold, with the majority of cases producing a reduced χ^2 less than unity, and occasionally greater than unity where the distributions within the parameterised spectrum are unable to represent a solution that matches the reaction rates.

Each unfolding method improved on the *a priori* given in most cases, with the energy regions where the subroutines tended to over or under predict being replicated in the behaviour of each unfolding method.

In the 1 - 20 MeV region each of the subroutines improved on the mean fractional deviation for most spectra and produced broadly similar results for the shape of the fusion peaks, an example of which is shown in the 'JET DT' spectrum in figure 3. The UF_M and UF_G subroutines performed most favourably, but by a relatively small margin, with UF_M and UF_G producing the lowest mean fractional deviation in 4/10 and 5/10 of the categories respectively. The percentage difference in integrated flux in this region was broadly similar for each method and to that of the *a priori* spectra.

The Gaussian used in the parameterised method to estimate the fusion peaks does not take into account the slight skew towards the lower energy caused by down-scatter of neutrons as they interact with material in the device. It is possible to improve the parameterised subroutine in future work by including a skewed normal distribution, keeping the skewing parameters free to allow a better fit to be found. It may be difficult to make a case for which type of skew may best represent this as the down-scatter will be heavily dependent on the medium the neutrons travel through before reaching the activation foil. As this skew was not accounted for, the subroutine tended to increase the width of the peak to compensate for this. Therefore, over estimating towards the higher energy side of the peak as shown in figure 4.

Between the fusion peaks (DD, DT or TT) and 1 MeV the subroutines tended to perform less favourably due to the region having a less smooth shape, which was not well approximated using the set of log-normal distributions, an example of which is shown in the calculated over target (C/T) plot, in figure 3.

In the 10^{-5} to 1 MeV region each of the subroutines showed best agreement with the integrated flux, with UF_M and the parameterised subroutine fitting well to the relatively smooth shape of this region. The UF_G subroutine also per-

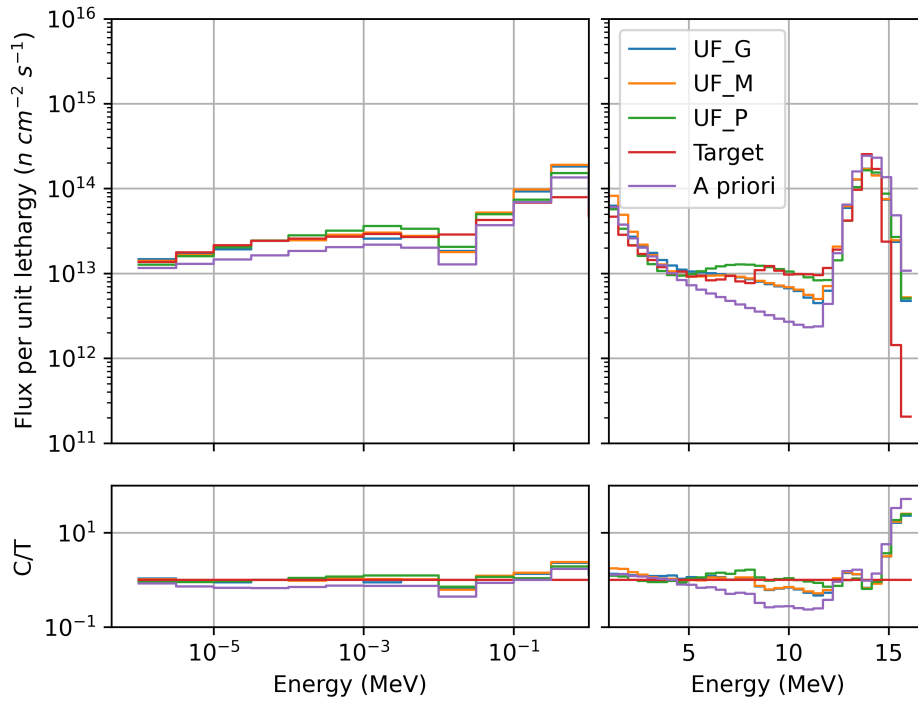


Figure 3: Target and solution spectra for the 'JET DT KN1 Octant 8' spectrum. C/T represents the ratio of the calculated solution to the target spectrum.

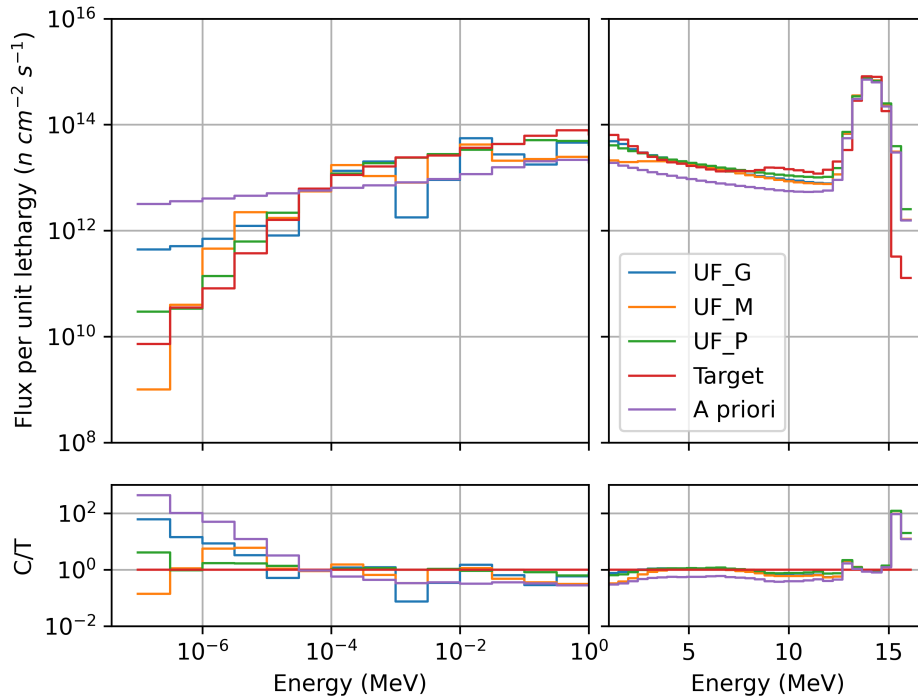


Figure 4: Target and solution spectra for the 'DEMO DT HCPB' spectrum. C/T represents the ratio of the calculated solution to the target spectrum.

Table 5

The mean of the fractional deviation of the solution flux from their respective target flux for each category of spectra and across the three energy regions of interest.

| Category | Method | 0 - 10^{-5} MeV | 10^{-5} - 1 MeV | 1 - 20 MeV | Total |
|------------------|----------|-------------------|-------------------|------------|---------|
| DT FW | UF_M | 0.711 | 0.412 | 11.599 | 7.907 |
| | UF_G | 32.777 | 9.407 | 11.884 | 13.979 |
| | UF_P | 35.847 | 79.244 | 19.441 | 33.951 |
| | A priori | 163.960 | 81.847 | 12.254 | 45.716 |
| DD | UF_M | 0.398 | 0.186 | 0.898 | 0.668 |
| | UF_G | 0.359 | 0.186 | 0.865 | 0.640 |
| | UF_P | 0.355 | 0.180 | 0.557 | 0.444 |
| | A priori | 0.442 | 0.193 | 2.332 | 1.588 |
| DT VV no water | UF_M | 1.419 | 0.265 | 0.700 | 0.699 |
| | UF_G | 1600.070 | 0.410 | 0.758 | 213.922 |
| | UF_P | 110.364 | 0.131 | 1.110 | 15.460 |
| | A priori | 4137.998 | 0.488 | 3.896 | 554.352 |
| DT VV with Water | UF_M | 0.287 | 0.240 | 0.523 | 0.429 |
| | UF_G | 0.331 | 0.378 | 0.717 | 0.590 |
| | UF_P | 3.643 | 1.440 | 1.304 | 1.646 |
| | A priori | 3.641 | 1.619 | 1.205 | 1.622 |
| DD KN1 | UF_M | 0.064 | 0.105 | 0.284 | 0.153 |
| | UF_G | 0.111 | 0.125 | 0.136 | 0.127 |
| | UF_P | 0.096 | 0.131 | 0.209 | 0.149 |
| | A priori | 0.719 | 0.352 | 0.398 | 0.409 |
| DT KN1 | UF_M | 0.055 | 0.189 | 1.372 | 1.035 |
| | UF_G | 0.099 | 0.214 | 1.297 | 0.989 |
| | UF_P | 0.085 | 0.212 | 1.375 | 1.045 |
| | A priori | 0.149 | 0.305 | 2.473 | 1.861 |
| TT KN1 | UF_M | 0.069 | 0.183 | 0.181 | 0.174 |
| | UF_G | 0.122 | 0.196 | 0.240 | 0.217 |
| | UF_P | 0.089 | 0.263 | 0.249 | 0.243 |
| | A priori | 0.263 | 0.213 | 0.280 | 0.256 |
| DD KN2/OLTIS | UF_M | 0.119 | 0.166 | 0.255 | 0.186 |
| | UF_G | 0.250 | 0.178 | 0.139 | 0.175 |
| | UF_P | 0.271 | 0.172 | 0.142 | 0.175 |
| | A priori | 1.460 | 0.329 | 0.308 | 0.456 |
| DT KN2/OLTIS | UF_M | 0.088 | 0.146 | 0.343 | 0.285 |
| | UF_G | 0.222 | 0.192 | 0.236 | 0.220 |
| | UF_P | 0.280 | 0.184 | 0.322 | 0.271 |
| | A priori | 0.535 | 0.187 | 0.451 | 0.366 |
| TT KN2/OLTIS | UF_M | 0.093 | 0.141 | 0.242 | 0.197 |
| | UF_G | 0.220 | 0.192 | 0.236 | 0.220 |
| | UF_P | 0.280 | 0.184 | 0.322 | 0.271 |
| | A priori | 0.535 | 0.187 | 0.451 | 0.366 |

formed well in this region. However, it did tend to make less adjustment to the *a priori* given and hence, the solution was much more dependent on the *a priori* given. Each of the methods also improved on the mean fractional deviation within most categories, with the UF_M method producing the most improvement on the *a priori* spectrum.

In the sub- 10^{-5} MeV region the UF_M subroutine performed most favourably by some margin, producing the most improvement in both the integrated flux and the mean fractional deviation as it was most able to approximate the steep

down-scatter slopes close to the thermal energies. Whereas, the parameterised subroutine was bound by the series of log-normal distributions and was less able to deviate from the relatively smooth shape and approximate the steeper slopes, possibly due to the rigidity of the logarithmically distributed log-normal distributions allowing only a relatively smooth line in logarithmic space. In contrast, the UF_M subroutine was able to move individual channels to make the most of the information provided. The UF_G subroutine once again made the least adjustment to the *a priori* out of each of the

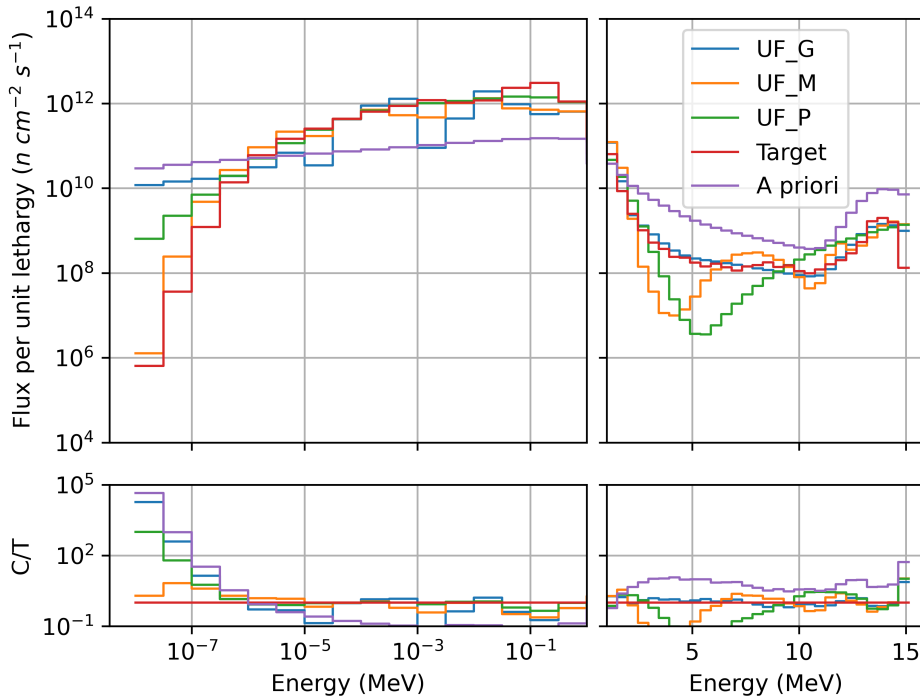


Figure 5: Target and solution spectra for the 'DT HCLL' spectrum. C/T represents the ratio of the calculated solution to the target spectrum. In this case the fit is less sensitive to the thermal (<0.1 eV) component of the spectrum resulting in significant variability in the unfolding results

subroutines and thus, struggled to fit to this region, particularly where the *a priori* was less accurate.

Where the shape of the *a priori* spectra had deviated from the target spectrum, each of the subroutines tended to behave poorly and show less agreement. This was especially the case where spectral flux spanned 6-7 orders of magnitude between the fusion peaks and the thermal region. This is partly due to the contribution of these regions to the reaction rate being relatively small compared to other regions, meaning the fitting in these regions tended to be less sensitive to changes in the solution spectrum. An example of this is shown in figure 5.

6. Conclusion

A modern combined framework of unfolding methods, SPECTRA-UF, was developed by UKAEA and tested, and a comparison of the UF_M, UF_G and UF_P subroutines was undertaken using a synthetic data set created from a range of fusion environments. The UF_P subroutine was used to generate *a priori* for each category of spectra within the comparison.

The SPECTRA-UF unfolding framework was written in Python 3 to aid the development and testing of activation foil systems for use in experiments and future applications in JET, ITER and DEMO. One main aim in the development of the framework is to allow for convenient processing of data

and the automation in application of each unfolding method, along with plotting and post processing of results.

A set of synthetic reaction rate data was created using DD, DT and TT spectra collected from or calculated using models of the JET, ITER and DEMO reactors. The response matrix created contained 11 reaction channels based on foils found in previous experimental work. A 56 energy group structure was used, with 16 relatively coarse logarithmically distributed lower energy bins, and 40 finer linearly distributed upper energy bins up to 20 MeV. This synthetic set of data was applied to the three unfolding methods.

When given *a priori* close to the target spectra, each of the subroutines behave in a similar fashion and will tend to over or under-predict the spectra in similar energy regions. Each method produced spectra with a similar total integrated flux, which on average deviated from the target spectra by between 8.3 % and 12.6 % across all spectra tested. The UF_M subroutine showed the lowest mean fractional deviation across all spectra and energy region. It was better able to fit to the steeper sloped regions found at lower energies in comparison to the parameterised and UF_G methods. The UF_G subroutine fitted well to the 1 - 20 MeV energy regions, but tended to make the least adjustment to the *a priori* spectrum in others and hence, was most sensitive to a *a priori* that deviated from the target spectra. Where the *a priori* deviated further from the target spectra, the subroutines tended to behave less predictably and tended to show less agree with

one another.

The use of a parameterised spectrum shows some promise, however, some underlying issues exist, such as the skewing of the fusion peaks towards lower energies, which will be improved in future work. The relatively smooth regions of the spectrum between 10^{-8} and 1 MeV were well approximated using the evenly logarithmically distributed set of log-normal distributions. However, these were less able to approximate the steeper regions, typically between 10^{-8} and 10^{-4} MeV. The use of the parameterised subroutine as an addition to the existing GRAVEL and MAXED methods may help the user check the reliability of the solution spectra provided, as with poorer *a priori*, each of the methods tended to produce differing solutions.

7. Acknowledgement

This work was funded by the RCUK Energy Programme [grant number EP/T012250/1].

References

- [1] Barros, S., Mares, V., Bedogni, R., Reginatto, M., Esposito, A., F. Gonçalves, I., Vaz, P., Rühm, W., 2014. Comparison of unfolding codes for neutron spectrometry with Bonner spheres. *Radiation Protection Dosimetry* 161, 46–52. doi:10.1093/rpd/nct353.
- [2] Basunia, M.S., 2018. Nuclear data sheets for $a=59$. *Nuclear Data Sheets* 151, 1 – 333. URL: <http://www.sciencedirect.com/science/article/pii/S0090375218300590>, doi:<https://doi.org/10.1016/j.nds.2018.08.001>.
- [3] Brackenbush, L.W., Scherpelz, R.I., 1984. Spectrum unfolding using information theory.
- [4] Brown, D., Chadwick, M., Capote, R., Kahler, A., Trkov, A., Herman, M., Sonzogni, A., Danon, Y., Carlson, A., Dunn, M., Smith, D., Hale, G., Arbanas, G., Arcilla, R., Bates, C., Beck, B., Becker, B., Brown, F., Casperson, R., Conlin, J., Cullen, D., Descalle, M.A., Firestone, R., Gaines, T., Guber, K., Hawari, A., Holmes, J., Johnson, T., Kawano, T., Kiedrowski, B., Koning, A., Kopecky, S., Leal, L., Lestone, J., Lubitz, C., Damián, J.M., Mattoon, C., McCutchan, E., Mughabghab, S., Navratil, P., Neudecker, D., Nobe, G., Noguere, G., Paris, M., Pigni, M., Plompen, A., Pritychenko, B., Pronyaev, V., Roubtsov, D., Rochman, D., Romano, P., Schillebeeckx, P., Simakov, S., Sin, M., Sirakov, I., Sleaford, B., Sobes, V., Soukhovitskii, E., Stetcu, I., Talou, P., Thompson, I., van der Marck, S., Welsch-Sherrill, L., Wiarda, D., White, M., Wormald, J., Wright, R., Zerkle, M., Žerovnik, G., Zhu, Y., 2018. ENDF/B-VIII.0: The 8th major release of the nuclear reaction data library with CIELO-project cross sections, new standards and thermal scattering data. *Nuclear Data Sheets* 148, 1 – 142. URL: <http://www.sciencedirect.com/science/article/pii/S0090375218300206>, doi:<https://doi.org/10.1016/j.nds.2018.02.001>. special Issue on Nuclear Reaction Data.
- [5] Browne, E., Tuli, J., 2013. Nuclear data sheets for $a = 60$. *Nuclear Data Sheets* 114, 1849 – 2022. URL: <http://www.sciencedirect.com/science/article/pii/S0090375213000823>, doi:<https://doi.org/10.1016/j.nds.2013.11.002>.
- [6] Byrd, R., Lu, P., Nocedal, J., Zhu, C., 1995. A limited memory algorithm for bound constrained optimization. *SIAM Journal of Scientific Computing* 16, 1190–1208. doi:10.1137/0916069.
- [7] Colling, B., Batistoni, P., Bradnam, S., Ghani, Z., Gilbert, M., Nobs, C., Packer, L., Pillon, M., Popovichev, S., 2018. Testing of tritium breeder blanket activation foil spectrometer during JET operations. *Fusion Engineering and Design* 136, 258 – 264. URL: <http://www.sciencedirect.com/science/article/pii/S0920379618301066>, doi:<https://doi.org/10.1016/j.fusengdes.2018.02.005>. special Issue: Proceedings of the 13th International Symposium on Fusion Nuclear Technology (ISFNT-13).
- [8] Dong, Y., Junde, H., 2014. Nuclear data sheets for $a = 54$. *Nuclear Data Sheets* 121, 1 – 142. URL: <http://www.sciencedirect.com/science/article/pii/S0090375214006553>, doi:<https://doi.org/10.1016/j.nds.2014.09.001>.
- [9] Ertek, C., 1985. Comparison of the SAND-II and LOUHI computer programs in unfolding neutron flux density spectra. *Nuclear Science and Engineering* 89, 191–195. URL: <https://www.scopus.com/inward/record.uri?eid=2-s2.0-0022011748&partnerID=40&md5=5d66b6d95a5924193efd69b26f5c38c8>. cited By 0.
- [10] Lengar, I., Žohar, A., Batistoni, P., Popovichev, S., Conroy, S., 2019. Characterization of JET neutron field in irradiation locations for DD, DT and TT plasmas. *Fusion Engineering and Design* 146, 1967 – 1970. URL: <http://www.sciencedirect.com/science/article/pii/S0920379619303953>, doi:<https://doi.org/10.1016/j.fusengdes.2019.03.078>. sl:SOFT-30.
- [11] Matzke, M., 1994. Unfolding of pulse height spectra : the HEPRO program system. Technical Report. Physikalisch-Technische Bundesanstalt.
- [12] Matzke, M., 2003. The HEPROW Program System. Technical Report. Physikalisch-Technische Bundesanstalt.
- [13] McCutchan, E., Sonzogni, A., 2014. Nuclear data sheets for $a = 88$. *Nuclear Data Sheets* 115, 135 – 304. URL: <http://www.sciencedirect.com/science/article/pii/S009037521300094X>, doi:<https://doi.org/10.1016/j.nds.2013.12.002>.
- [14] McElroy, W., Berg, S., Crockett, T., Hawkins, R., 1967. A Computer-Automated Iterative Method for Neutron Flux Spectra Determination by Foil Activation. Technical Report. United States Air Force.
- [15] Nesaraja, C.D., Geraedts, S.D., Singh, B., 2010. Nuclear data sheets for $a = 58$. *Nuclear Data Sheets* 111, 897 – 1092. URL: <http://www.sciencedirect.com/science/article/pii/S0090375210000359>, doi:<https://doi.org/10.1016/j.nds.2010.03.003>.
- [16] Nobs, C., Packer, L., Batistoni, P., Colling, B., Ghani, Z., Gilbert, M., Loret, S., Mergia, K., Messoloras, S., Michelakaki, I., Pillon, M., Savva, M., Stamatelatos, I., Triantou, K., Vasilopoulou, T., 2019. Neutron spectrum unfolding for the development of a novel neutron detector for fusion. *Fusion Engineering and Design* 146, 2658 – 2662. URL: <http://www.sciencedirect.com/science/article/pii/S0920379619306088>, doi:<https://doi.org/10.1016/j.fusengdes.2019.04.074>. sl:SOFT-30.
- [17] Packer, L., Batistoni, P., Bradnam, S., Colling, B., Conroy, S., Ghani, Z., Gilbert, M., Jednorog, S., Łaszyńska, E., Leichte, D., Lengar, I., Mieltski, J., Misiak, R., Nobs, C., Pillon, M., Popovichev, S., Radulović, V., Stamatelatos, I., Vasilopoulou, T., and A.W.G., 2018. Activation of ITER materials in JET: nuclear characterisation experiments for the long-term irradiation station. *Nuclear Fusion* 58, 096013. URL: <https://doi.org/10.1088/1741-4326/58/2/aacca0>, doi:10.1088/1741-4326/aacca0.
- [18] Reginatto, M., Goldhagen, P., 1998. MAXED, a computer code for the deconvolution of multisphere neutron spectrometer data using the maximum entropy method. Technical Report. Environmental Measurements Laboratory.
- [19] Routti, J.T., Sandberg, J.V., 1980. General purpose unfolding program LOUHI78 with linear and nonlinear regularizations. *Computer Physics Communications* 21, 119–144. doi:10.1016/0010-4655(80)90081-8.
- [20] scipy.org, 2020. Scipy basin hopping optimisation algorithm. <https://docs.scipy.org/doc/scipy/reference/generated/scipy.optimize.basinhopping.html>.
- [21] Singh, B., 2015. Nuclear data sheets for $a = 182$. *Nuclear Data Sheets* 130, 21 – 126. URL: <http://www.sciencedirect.com/science/article/pii/S0090375215000563>, doi:<https://doi.org/10.1016/j.nds.2015.11.002>.
- [22] Tsotridis, G., Dierckx, R., D’Hondt, P., 1992. Seventh ASTM-EURATOM Symposium on Reactor Dosimetry.
- [23] UKAEA, 2020. FISPACT-II reference input spectra. https://fispact.ukaea.uk/wiki/Reference_input_spectra.

- [24] Vasilopoulou, T., Stamatelatos, I., Batistoni, P., Colangeli, A., Flammini, D., Fomesu, N., Loreti, S., Obryk, B., Pillon, M., Villari, R., 2019. Improved neutron activation dosimetry for fusion. *Fusion Engineering and Design* 139, 109 – 114. URL: <http://www.sciencedirect.com/science/article/pii/S092037961930002X>, doi:<https://doi.org/10.1016/j.fusengdes.2019.01.002>.
- [25] Wang, Z., Kry, S.F., Howell, R.M., Salehpour, M., 2009. Comparison of unfolding methods for determining neutron spectrum and ambient dose equivalent. *Nuclear Technology* 168, 610–614. URL: <https://doi.org/10.13182/NT09-A9277>, doi:10.13182/NT09-A9277.
- [26] Wu, S.C., 2000. Nuclear data sheets for $a = 46$. *Nuclear Data Sheets* 91, 1 – 116. URL: <http://www.sciencedirect.com/science/article/pii/S0090375200900140>, doi:<https://doi.org/10.1006/ndsh.2000.0014>.